Modeling Land Cover Impact on Albedo Changes in Google Earth Engine Environment

Alessandra Capolupo(✉), Cristina Monterisi, Alberico Sonnessa, Giacomo Caporusso, and Eufemia Tarantino

Department of Civil, Environmental, Land, Construction and Chemistry (DICATECh), Politecnico di Bari, Via Orabona 4, 70125 Bari, Italy
alessandra.capolupo@poliba.it

Abstract. Over the last decades, Earth's surface has suffered an intense urbanisation process that has impacted Land Use/Land Cover (LULC) and Earth's surface energy balance. Such a rapid and unexpected phenomenon was not carried out in a sustainable way compromising Earth's existence in the long term. Therefore, the United States identified 17 Sustainable Development Goals (SDGs) to meet within 2030. To make the world more resilient and sustainable and combat climate changes, information concerning LULC conversion trends and land surface albedo is essential. Such variables are directly responsible for the increment and decrement of air and surface temperature and, consequently, to the Urban Heat Island (UHI) phenomenon. The present paper explores Google Earth Engine (GEE) platform potentialities in investigating the relationship between LULC transformation and land surface albedo extracted from medium-resolution satellite data. The present analysis was performed on the study area of Berlin for 8 years, from 2011 to 2019. Two radiometrically and atmospherically corrected Landsat images were gathered from Landsat 5 and Landsat 8 missions, respectively. Once clouds have been masked, SwirTirRed (STRed) and Normalized Difference Bareness (version 1) (NDBaI1) indices were implemented to distinguish LULC types. Subsequently, LULC changes were assessed, and land surface albedo was estimated by programming a proper code. Thus, the relationship among those features was investigated in such areas in the considered period. GEE appears as the optimal solution to meet research goals and to extend the analysis at a global scale.

Keywords: Geospatial big data · Sustainable development · Urban Heat Island · Climate change · Landsat satellite images

1 Introduction

Environmental ecosystem degradation and human well-being reduction are mainly due to global warming, which is enhanced by anthropogenic activities [1, 2]. Urbanisation phenomenon, indeed, defaces natural Land Use/Land Cover (LULC) and this directly impacts on Earth's surface energy balance of such area [3–8] and, consequently, on its air and surface temperatures. The wide use of non-evaporating impervious materials in the

© Springer Nature Switzerland AG 2021
O. Gervasi et al. (Eds.): ICCSA 2021, LNCS 12955, pp. 89–101, 2021.
https://doi.org/10.1007/978-3-030-87007-2_7

built environment is one of the main factors causing the Urban Heat Island (UHI) phenomenon [9], which describes the higher air and surface temperatures in built-up areas in comparison to surrounding rural environments [10]. This issue is further intensified by the unchecked, unsustainable urban sprawl that occurred in the last few years.

To face such a situation and to improve cities sustainability and resilience to climate changes, the United States detected 17 Sustainable Development Goals (SDGs) to meet within 2030. Thus, LULC transformation and albedo changes are the main driving forces to be investigated in order to address the SDGs [11, 12]. Well-defined indices to detect such features globally and locally and to explore their relationship are needed. Among the various techniques developed over the years, Remote Sensing is a powerful tool to accurately quantify them in a short time [13, 14]. According to study areas characteristics and variables to analyse, different approaches may be adopted. Each of them requires a different amount of a priori information and a specific processing time, allowing to achieve a given accuracy. Thus, the optimal strategy should be selected as a compromise among resultant map accuracy, processing time and algorithms complexity to be implemented [15]. For instance, LULC classes extraction is commonly carried out using one of the following approaches: Maximum Likelihood (ML) [16], Index-Based approach (IB) [17], Object-Based Image Analysis (OBIA) [17–19], Machine Learning Algorithms (MLA) [20]. Nonetheless, each of them shows some weakness: ML achieves the lowest accuracy [21], IB involves the application of several indices to classify a large area [15], OBIA requires a huge number of a priori information [22], and, lastly, MLA are based on very complex algorithms [20].

The estimation of land surface albedo is still difficult to derive from satellite images. Satellites, cannot measure such parameter directly and, therefore, over the years, several algorithms, consistent with sensor features mounted on the applied platforms, have been proposed. Nevertheless, all of them are based on Top Of the Atmosphere (TOA) corrected images because of the need to remove the atmospheric scattering inferring with the surface albedo [23].

Defining LULC trends and albedo changes over the years is time-consuming since a considerable number of geospatial data covering a large interval should be handled. Just the introduction of cloud-based platforms allowed to meet such emerging needs. Therefore, Google Earth Engine (GEE) environment has appeared as a good solution to process big geospatial data provided by several sources [24]. A proper infrastructure, a storage unit, daily updated with nearly free-available 6000 raw and pre-processed data, and a python/JavaScript-based Application Programming Interface (API) are its main components [25]. Mainly, API makes it more flexible than traditional desktop system because it ensures the opportunity to exploit complex and advanced algorithms already implemented in GEE libraries or to program new ones [24, 25].

Additionally, it allows minimising processing time thanks to many processors working in parallel. Hansen et al. (2013) [26] demonstrated the time needed to track forest cover changes between 2000 and 2012 by processing 654,178 Landsat 7 scenes (707 terabytes) was of 100 h and 1,000,000 h in GEE and desktop system, respectively. Such an experiment confirmed the substantial improvements introduced by GEE platform in the remote sensing world. Nevertheless, a significant effort is still needed to develop good algorithms to produce accurate classification and land surface albedo maps.

The present research is framed in such a context. This study is aimed at developing a proper Javascript code in GEE environment to analyse: i) LULC transformation over 8 years, from 2011 up to 2019; and ii) land surface albedo trends over the same period. Lastly, the relationship between such phenomena was explored too. The municipality of Berlin was selected as a pilot case. Both features were extracted from medium-resolution Landsat satellite images belonging to mission 5 and 8.

2 Material and Methods

2.1 Area of Interest and Selected Data

Berlin city, located in the eastern part of Germany, was selected as the experimental site to investigate the impact of LULC variation on land surface albedo (Fig. 1). Such area was characterised by a significant urban sprawl between 2011 and 2019. This phenomenon was enhanced by the flat topography of such zone as well as economic interests. Indeed, an average inhabits increment equal to 16% per year in the residential zone was detected [27]. Simultaneously, new projections indicate a continuous population growth in the inner area within 2030.

Nonetheless, currently, it is one of the greenest cities in the world, thanks to the presence of large public green spaces and forested areas. Such features cover about the 30% of the whole territory [28]. Because of the above-mentioned properties, it was considered as the optimal site to meet the research purposes.

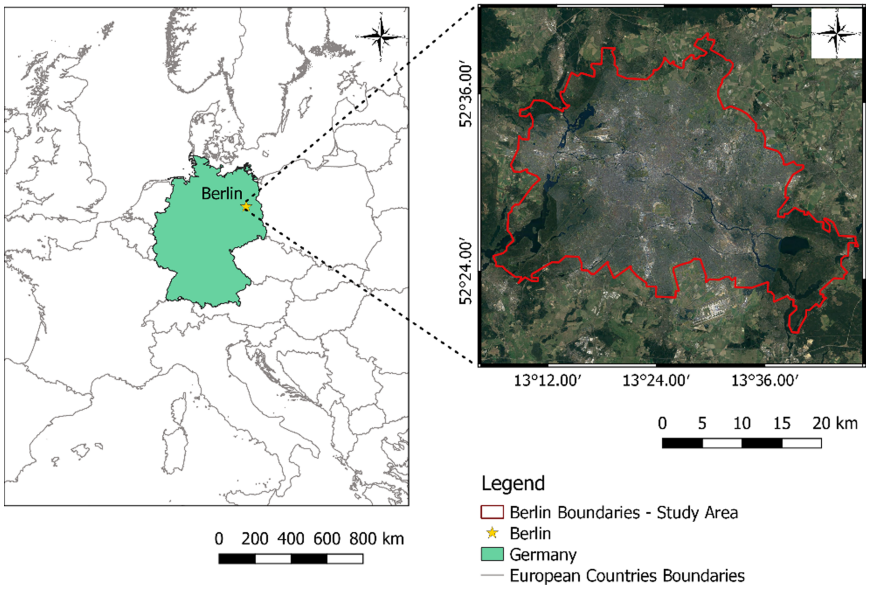

Fig. 1. Overview of the study area. Germany position in the European context on the left and zoom on Berlin city on the right. (Color figure online)

2.2 Operative Workflow and Database Construction

Figure 2 reports the operative workflow adopted to meet the research purposes. Once selecting satellite data and constructing the geo-database, images quality was assessed and improved. Such pre-processed data were used as input of the subsequent processing investigations. Firstly, LULC classification map was extracted through the computation of proper vegetation indices. Simultaneously, the land surface albedo was estimated too. Lastly, before statistically investigating the correlation among the outputs of previous processing steps, the reliability of such findings was investigated. Each phase is detailed in what follows.

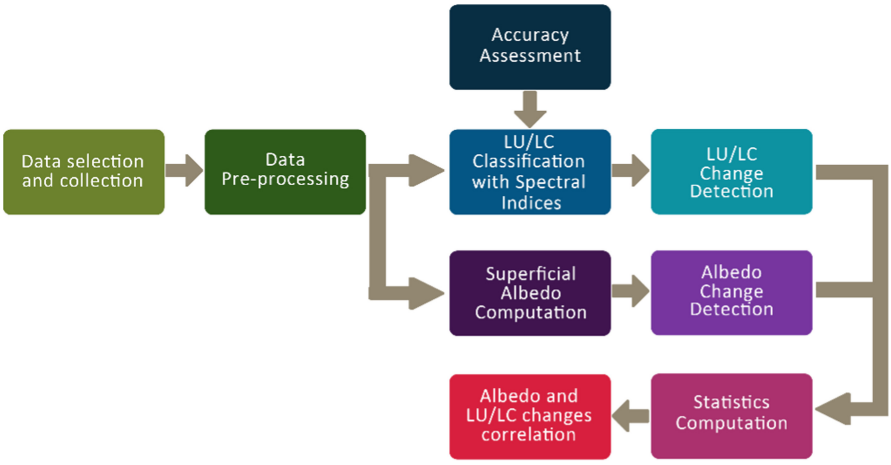

Fig. 2. Operative workflow to investigate the impact of LULC transformation on albedo changes.

All phases of the above-mentioned operative workflow were implemented in the GEE environment by developing a proper Javascript code. Thanks to the integrated catalogue, users can access both raw and pre-processed data, importing them in the API directly without needing to download them locally. This property contributes to reducing collecting and operational time [27] drastically.

Thus, two atmospherically corrected Landsat images belonging to missions 5 and 8 were picked up from the storage unit and imported in the API. The image selection was performed considering two main factors: acquisition time and cloud cover. To detect the changes without considering the impact of different seasons, only the images gathered in the same month, June, were analysed. Conversely, to minimise the cloud coverage influence, a threshold equal to 15% was set. Although both data met such requirement (Table 1), as suggested by [30], the clouds in Landsat 8 image were subsequently filtered. The orthorectification phase, instead, was not carried out since the data quality was satisfying. More details about data features are reported in Table 1. This dataset was further investigated in the subsequent steps.

Table 1. Main features of selected Landsat data. TM: thematic mapper; OLI-TIRS: operational land imager - thermal infrared.

ID	Landsat Mission	Sensor	Landsat Images	Acquisition Date (mm/dd/yyyy)	Acquisition Time	Average Cloud Cover (%)
1	Landsat 5	TM	LT05_L1TP_193023_20110602_20161009_01_T1	06/02/2011	09:52	0
2	Landsat 8	OLI-TIRS	LC08_L1TP_193023_20190624_20190704_01_T1	06/24/2019	10:02	12

2.3 LULC Classification and Change Detection Analysis and Accuracy Assessment

Index-based methods are commonly applied to quickly produce thematic maps of a certain area, albeit each index can automatically get just a few LULC classes. Therefore, the combination of more indices is often required to classify the whole experimental site. This was the case of the present research where the version 1 of the Normalized Difference Bareness Index (NDBaI1) (Eq. 1) [31] and the SwirTirRed (STRed) index (Eq. 2) [32] were integrated.

$$NDBaI1 = \frac{SWIR2 - TIR1}{SWIR2 + TIR1} \tag{1}$$

$$STRed = \frac{SWIR1 + R - TIR1}{SWIR1 + R + TIR1} \tag{2}$$

NDBaI1 allowed detecting bare soil and built-up classes, as well as STRed, by permitting to distinguish water, dense and sparse vegetation. This procedure was separately implemented on both pre-processed images.

The accuracy of the resultant maps was assessed by computing three widely applied statistical metrics: i) the Overall Accuracy (OA), ii) the Producer's Accuracy (PA), and, lastly, iii) the User's Accuracy (UA) [33, 34]. All of them can assume a value comprised between 0 and 1. The highest the value, the most accurate the finding is. These indicators were calculated by comparing the obtained thematic maps with a reference set of 40068 testing pixels, generated using the "stratified random sampling polygon" approach [35]. A testing sample number consistent with the classes size was selected. Thus, 5354, 14063, 4302, 4179, and, lastly, 12170 were picked up from water, dense vegetation, sparse vegetation, built-up and bare soil categories, respectively.

2.4 Land Surface Albedo Computation

In 2000, Liang et al. [36] developed various processes to estimate the land surface albedo from different satellite platforms. They handled the most widely spread satellite images at that time, like Landsat, using hundreds of filed measurements as calibration data. Equation 3 reports the formula to compute the albedo (a) from Landsat images:

$$a = 0.356 * \varrho_1 + 0.130 * \varrho_3 + 0.373 * \varrho_4 + 0.085 * \varrho_5 + 0.072 * \varrho_7 - 0.0018 \quad (3)$$

ϱ_i are the Top of Atmosphere (ToA) Landsat bands.
This formula was, subsequently, snormalised by Smith et al. (2000) [37] (Eq. 4).

$$a = \frac{0.356 * \varrho_1 + 0.130 * \varrho_3 + 0.373 * \varrho_4 + 0.085 * \varrho_5 + 0.072 * \varrho_7 - 0.0018}{0.356 + 0.130 + 0.373 + 0.085 + 0.072} \quad (4)$$

Equation 4 was implemented in the GEE environment to compute a from the two Landsat images.

2.5 Change Detection Analysis and Relationship Between LULC and Albedo

A multitemporal analysis over a period of 8 years considering both LULC and a was performed. Although various methods have been developed, the approach based on the comparison of the resultant thematic maps was preferred. Indeed, this time-saving approach allows detecting the altered areas without using a hard computational power [38]. It involves the subtraction of a thematic map from that one produced on the previous date. Equations 5 and 6 report the formula to compute the LULC and a changes, respectively.

$$CD_{LULC} = LULC_2 - LULC_1 \quad (5)$$

where $LULC_2$ and $LULC_1$ are the LULC maps generated from the images collected in 2019 and 2011, respectively.

$$CD_a = a_2 - a_1 \quad (6)$$

where a_2 and a_1 are the albedo charts produced from the Landsat images acquired in 2019 and 2011, respectively.

This approach does not suffer from topographic characteristics influence, and, consequently, it may be applied in all LULC environment [39]. Nevertheless, the accuracy of its outcomes is affected by the random noise [39]. Thus, the variation percentage of both parameters was computed for each LULC class.

Once the change detection analysis was completed, the correlation between the two resultant maps was carried out. This step was essential to analyse the influence of LULC alteration on surface energy balance.

3 Results and Discussion

Figure 3 reports the outcome of the index-based method, separately applied on the input set of data. As previously described, it was generated by computing the STRed and the NDBaI1 indices. The former detected water, sparse and dense vegetation, while the latter distinguished bare soil and built-up zone. Although this method does not allow quantitatively detecting the changes occurring in such a site, it permits a preliminary idea of the transformation process. Thus, a visual inspection of the resultant thematic maps was performed as well as the area covered by each LULC category was computed. These steps provided information regarding the relevant urban sprawl phenomenon that occurred around the city centre and the increment of the green areas in the peri-urban areas. Indeed, the number of red and green pixels is higher in the middle and on the border of the Landsat images acquired on the 24th of June 2019 (Fig. 3D) than the one collected on the 2nd of June 2011.

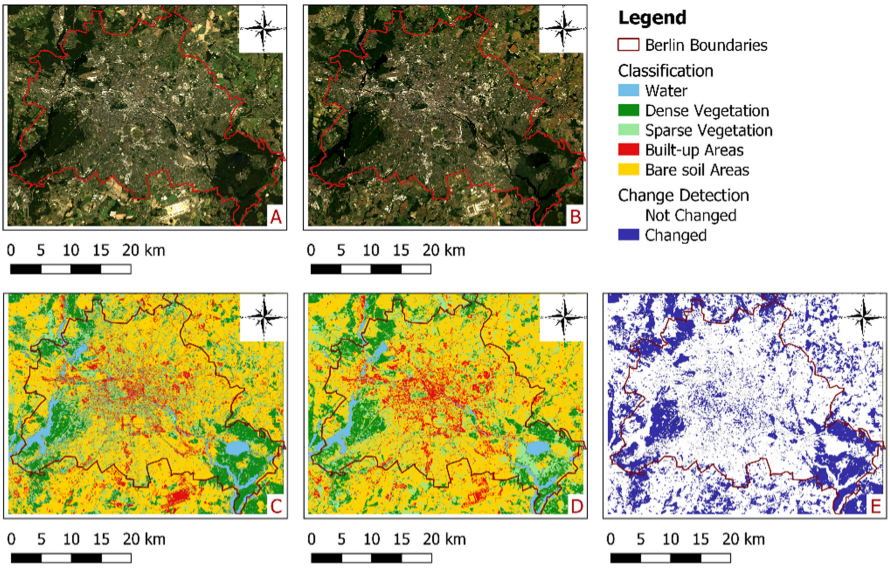

Fig. 3. Landsat data acquired by missions five on 2nd of June 2011 (A) and eight on 24th of June 2019 (B); the corresponding LULC classifications in (C) and (D); and LULC changes occurred between 2011 and 2019 (E). (Color figure online)

Nevertheless, considering the whole study area, an urban zone and bare soil extension reduction were identified (Table 2). Conversely, sparse and dense vegetated pixels covered a higher extended area. This analysis was subsequently detailed during the change detection investigation phase.

Table 2. LULC classes extension extracted by handling satellite images acquired by Landsat missions 5 and 8, respectively.

LU/LC Class coverage	L5 - 06/02/2011	L8 - 06/24/2019
Water (%)	3.38	3.58
Dense Vegetation (%)	15.21	15.76
Sparse Vegetation (%)	16.76	17.46
Built-up (%)	5.42	5.25
Bare soil (%)	59.23	57.95

Before proceeding with the change detection phase, STRed and NDBaI1 accuracy was evaluated. Indeed, such indices were selected according to their effectiveness shown in the previous studies [17, 29, 31]. Metrics accuracy, reported in Table 3, confirms their reliability in extracting LULC information. Indeed, their OA is equal to 89.78% and 90.06%, respectively. Nevertheless, the classification result is affected by STRed performance in classifying the sparse vegetation zone and by NDBaI1 ability in detecting built-up areas [29]. Indeed, PA and UA values of such groups are the smallest.

Table 3. Producer, user and overall accuracy of the two collected satellite images

	L5 - 06/02/2011		L8 - 06/24/2019	
Land Cover Class	PA (%)	UA (%)	PA (%)	UA (%)
Water	99.25	99.42	98.66	98.51
Dense Veg.	91.49	97.44	87.56	97.84
Sparse Veg.	83.26	64.18	83.24	36.9
Built-up	67.84	89.66	77.64	99.22
Bare soil	95.89	85.79	95.88	89.44
OA (%)	89.78		90.07	

On the basis of the accuracy results, the generated classification maps were considered reliable, and thus, they were applied in the subsequent investigation phase through the computation of CD_{LULC}. Figure 3E shows CD_{LULC} result: transformed and not transformed areas are described in blue and white, respectively. This analysis confirms the results obtained by the qualitative investigation. Although an urban sprawl phenomenon is visible, a substantial increment of the green areas is reported on the surrounding. Figure 3E allows spatially allocating the transformed zone, while Table 4 gives the conversion percentage. Most of the changes were in the urban and sparse vegetated areas. The former class was drastically reduced in favour of bare soil and sparse vegetation; conversely, the latter was partially converted in dense vegetation and partially in bare soil. The conversion of sparse green areas is mainly linked to the difficulties of STRed index in correctly classifying such group. Probably, the images acquisition period affected the

discrimination of such group too. Similarly, the scarce accuracy of NDBaI1 in detecting built-up areas compromised CD_{LULC} results too.

Table 4. LULC conversion over an investigated period of 8 years (2011–2019).

	L8 24/06/2019				
L5 02/06/2011	Water (%)	Dense Veg. (%)	Sparse Veg. (%)	Bare soil Areas (%)	Built-up Areas (%)
Water (%)	98.13	0.64	0.36	0.16	0.71
Dense Veg. (%)	1.25	73.37	20.19	4.85	0.34
Sparse Veg. (%)	0.04	33.74	35.63	28.51	2.09
Bare soil Areas (%)	0.01	0.51	8.78	88.39	2.31
Built-up Areas (%)	0.02	0.10	2.15	24.27	73.46

Figure 4 reports the land surface albedo obtained from the input pre-processed satellite images using the snormalised version of Liang et al. [36] algorithm. Visually comparing the two colour-graduated maps, an increment of the land surface albedo can be detected over the investigated period. Specifically, detected changes are reported in Fig. 4E. Thus, LULC and albedo transformations were correlated to sanalyse the impact of LULC changes on surface energy.

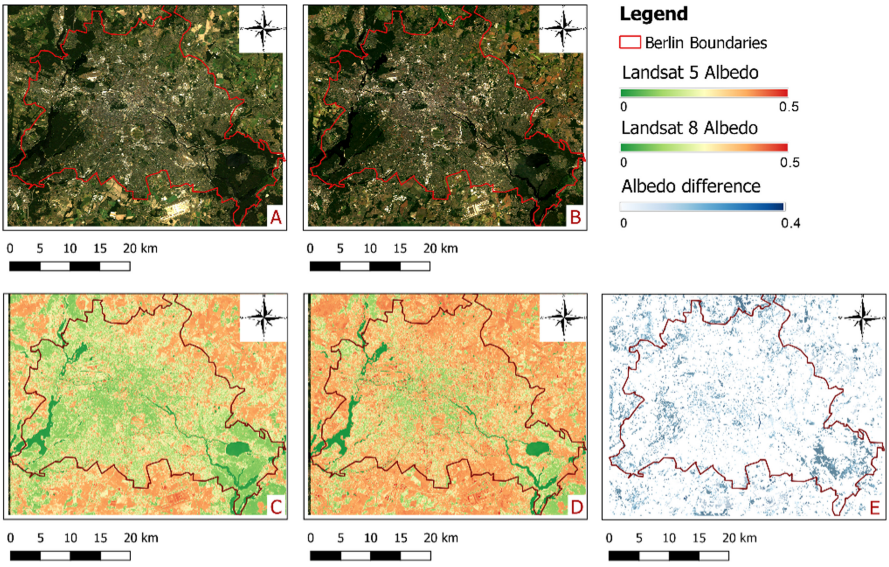

Fig. 4. Landsat data acquired by missions five on 2nd of June 2011 (A) and eight on 24th of June 2019 (B); the corresponding land surface albedo in (C) and (D); and land surface albedo changes occurred between 2011 and 2019 (E).

Both alterations are reported in Fig. 5, which shows the location correspondence between the two outcomes. Additionally, a substantial increment of albedo can be detected in those areas converted from dense to sparse vegetation or to bare soil. A slight increment, instead, is seen in the other cases. Figure 5 shows percentage variation too.

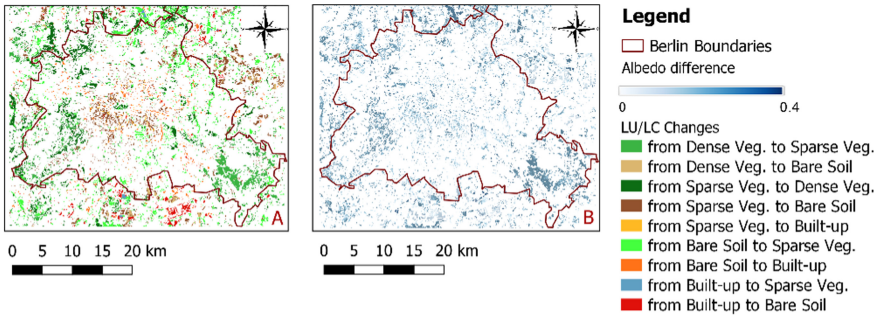

Class L5	Class L8	% of change
Dense Veg.	Sparse Veg.	20
Dense Veg.	Bare soil	5
Dense Veg.	Dense Veg.	34
Dense Veg.	Bare soil	29
Dense Veg.	Built-up	2
Bare soil	Sparse Veg.	9
Bare soil	Built-up	2
Built-up	Sparse Veg.	2
Built-up	Bare soil	24

Class L5	Class L8	Variation Albedo (%)
Dense Veg.	Sparse Veg.	33
Dense Veg.	Bare soil	-9
Sparse Veg.	Dense Veg.	18
Sparse Veg.	Bare soil	8
Sparse Veg.	Built-up	33
Bare soil	Sparse Veg.	19
Bare soil	Built-up	57
Built-up	Sparse Veg.	20
Built-up	Bare soil	-12

Fig. 5. LULC (A) and albedo (B) changes and the corresponding percentage variation in the tables at the bottom

4 Conclusion

The goal of this paper was to analyse LULC and albedo transformation processes that occurred over a period of about 8 years (2011–2019) in the pilot site of Berlin. Once the detection phase was concluded, the impact of LULC alteration on the surface energy balance was investigated. Berlin was selected as the pilot site of this work because of the urbanisation process that it suffered to address the strong population growth. Indeed, although berlin is still considered one of the greenest cities worldwide, a strong urban sprawl phenomenon can be detected in the urban areas. Conversely, green areas were further intensified in semi-urban zones. Nonetheless, considering the whole study area, the greenery conversion was more relevant than the urbanisation one. This did not imply a land surface albedo reduction, as expected, mainly because of the kind of vegetation introduced in the city. Most of the areas were characterised by sparse vegetation, and it is widely known that its albedo value is pretty like that of built-up areas. Thus, the adopted planning strategies were not suitable for improving the land surface albedo condition and tackling climate change issues.

All the investigation was performed in a GEE environment that appeared as an essential tool to meet the research purposes. Indeed, thanks to its great versatility, mainly due to the possibility to customise the algorithms; it allowed to build a proper Javascript code able to meet all the investigation steps. Additionally, being a cloud environment, it allows reducing the operational time overcoming standard desktop limitations.

Thus, combining the implemented operative workflow and GEE environment allows obtaining promising findings in detecting the impact of LULC transformation on albedo alteration. Thus, in the near future, such developed code will be applied worldwide to produce a thematic map to explore the linkage between such indicators.

Acknowledgements. This research is partially funded under the project "AIM1871082-1" of the AIM (Attraction and International Mobility) Program, financed by the Italian Ministry of Education, University and Research (MIUR).

References

1. Singh, A., Purohit, B.M.: Public health impacts of global warming and climate change. Peace Rev. **26**, 112–120 (2014)
2. Al-Ghussain, L.: Global warming: review on driving forces and mitigation. Environ. Prog. Sustain. Energy **38**, 13–21 (2019)
3. Boccia, L., Capolupo, A., Rigillo, M., Russo, V.: Terrace abandonment hazards in a mediterranean cultural landscape. J. Hazard. Toxic Radioact. Waste **24**(1), 04019034 (2020)
4. Lama, G.F.C., Chirico, G.B.: Effects of reed beds management on the hydrodynamic behaviour of vegetated open channels. In: 2020 IEEE International Workshop on Metrology for Agriculture and Forestry (MetroAgriFor), pp. 149–154. IEEE, November (2020)
5. Capolupo, A., Boccia, L.: Innovative method for linking anthropisation process to vulnerability. World Rev. Sci. Technol. Sustain. Dev. **17**(1), 4–22 (2021)
6. Errico, A., Lama, G.F.C., Francalanci, S., Chirico, G.B., Solari, L., Preti, F.: Flow dynamics and turbulence patterns in a drainage channel colonized by common reed (Phragmites australis) under different scenarios of vegetation management. Ecol. Eng. **133**, 39–52 (2019). https://doi.org/10.1016/j.ecoleng.2019.04.016
7. Apollonio, C., Balacco, G., Novelli, A., Tarantino, E., Piccinni, A.F.: Land use change impact on flooding areas: the case study of Cervaro Basin (Italy). Sustainability **8**(10), 996 (2016)
8. Lama, G.F.C., Crimaldi, M., Pasquino, V., Padulano, R., Chirico, G.B.: Bulk drag predictions of riparian arundo donax stands through UAV-acquired multispectral images. Water **13**(10), 1333 (2021). https://doi.org/10.3390/w13101333
9. Stathopoulou, E., Mihalakakou, G., Santamouris, M., Bagiorgas, H.S.: On the impact of temperature on tropospheric ozone concentration levels in urban environments. J. Earth Syst. Sci. **117**(3), 227–236 (2008)
10. Santamouris, M.: Urban reality – solar design and refurbishment in the built environment. United Kingdom (2001)
11. Voogt, J.A., Oke, T.R.: Thermal remote sensing of urban climates. Remote Sens. Environ. **86**, 370–384 (2003)
12. Souch, C., Grimmond, S.: Applied climatology: urban climate. Prog. Phys. Geogr. **30**, 270–279 (2006)
13. Chen, X.L., Zhao, H.M., Li, P.X., Yin, Z.Y.: Remote sensing image-based analysis of the relationship between urban heat island and land use/cover changes. Remote Sens. Environ. **104**(2), 133–146 (2006)

14. Mirzaei, M., Verrelst, J., Arbabi, M., Shaklabadi, Z., Lotfizadeh, M.: Urban heat island monitoring and impacts on citizen's general health status in Isfahan metropolis: a remote sensing and field survey approach. Remote Sens. **12**(8), 1350 (2020)
15. Patel, N., et al.: Multitemporalsettlement and population mapping from Landsat using Google Earth Engine. Int. J. Appl. Earth Obs. Geoinf. **35**(199–208), 2015 (2015)
16. Susaki, J., Shibasaki, R.: Maximum likelihood method modified in estimating a prior probability and in improving misclassification errors. Int. Arch. Photogramm. Remote Sens. **33**, 1499–1504 (2000)
17. Capolupo, A., Monterisi, C., Caporusso, G., Tarantino, E.: Extracting land cover data using GEE: a review of the classification indices. In: Gervasi, O., Murgante, B., Misra, S., Garau, C., Blečić, I., Taniar, D., Apduhan, B.O., Rocha, A.M.A.C., Tarantino, E., Torre, C.M., Karaca, Y. (eds.) ICCSA 2020. LNCS, vol. 12252, pp. 782–796. Springer, Cham (2020). https://doi.org/10.1007/978-3-030-58811-3_56
18. Crocetto, N., Tarantino, E.: A class-oriented strategy for features extraction from multidate ASTER imagery. Remote Sens. **1**, 1171–1189 (2009)
19. Sarzana, T., Maltese, A., Capolupo, A., Tarantino, E.: Post-processing of pixel and object-based land cover classifications of very high spatial resolution images. In: Gervasi, O., Murgante, B., Misra, S., Garau, C., Blečić, I., Taniar, D., Apduhan, B.O., Ana, M.A., Rocha, C., Tarantino, E., Torre, C.M., Karaca, Y. (eds.) Computational Science and Its Applications – ICCSA 2020: 20th International Conference, Cagliari, Italy, July 1–4, 2020, Proceedings, Part IV, pp. 797–812. Springer International Publishing, Cham (2020). https://doi.org/10.1007/978-3-030-58811-3_57
20. Praticò, S., Solano, F., Di Fazio, S., Modica, G.: Machine learning classification of mediterranean forest habitats in Google earth engine based on seasonal sentinel-2 time-series and input image composition optimisation. Remote Sens. **13**(4), 586 (2021)
21. Chen, J., Gong, P., He, C., Pu, R., Shi, P.: Land-use/land-cover change detection using improved change-vector analysis. Photogramm. Eng. Remote Sens. **69**, 369–380 (2003)
22. Whiteside, T.G., Boggs, G.S., Maier, S.W.: Comparing object-based and pixel-based classifications for mapping savannas. Int. J. Appl. Earth Obs. Geoinf. **136**, 884–893 (2011)
23. Li, Z., Garand, L.: Estimation of surface albedo from space: a parameterization for global application. J. Geophys. Res.: Atmos. **99**(D4), 8335–8350 (1994)
24. Gorelick, N., Hancher, M., Dixon, M., Ilyushchenko, S., Thau, D., Moore, R.: Google Earth Engine: planetary-scale geospatial analysis for everyone. Remote Sens. Environ. **202**, 18–27 (2017)
25. Kumar, L., Mutanga, O.: Google earth engine applications since inception: usage, trends, and potential. Remote Sens. **10**(10), 1509 (2018)
26. Hansen, M., et al.: Observing the forest and the trees: the first high resolution global maps of forest cover change. Science **342**, 850–853 (2013)
27. Amt für Statistik: Berlin-Brandenburg Statistik Berlin-Brandenburg (2019). http://www.statistik-berlin-brandenburg.de/home.asp. Accessed 10 May 2019
28. Senatsverwaltung für Stadtentwicklung und Umwelt Berlin Stadtentwicklungsplan Wohnen 2025, Berlin, p. 119 (2014). http://www.stadtentwicklung.berlin.de/planen/stadtentwicklungsplanung/de/wohnen/download/step_wohnen_2025_bericht.pdf
29. Capolupo, A., Monterisi, C., Saponaro, M., Tarantino, E.: Multi-temporal analysis of land cover changes using Landsat data through Google Earth Engine platform. In: Eighth International Conference on Remote Sensing and Geoinformation of the Environment (RSCy2020), vol. 11524, p. 1152419. International Society for Optics and Photonics, August (2020)
30. Kauth, R.J.; Thomas, G.S.: The tasselled cap—a graphic description of the spectraltemporal development of agricultural crops as seen by landsat. In: Symposium on Machine Processing of Remotely Sensed Data. Purdue University, West Lafayette, Indiana, pp. 41–51 (1976)

31. Li, S., Chen, X.: A new bare-soil index for rapid mapping developing areas using landsat 8 data. Int. Arch. Photogramm. Remote Sens. Spatial Inf. Sci. **40**, 139–144 (2014)
32. Capolupo, A., Monterisi, C., Tarantino, E.: Landsat Images Classification Algorithm (LICA) to automatically extract land cover information in Google earth engine environment. Remote Sens. **12**(7), 1201 (2020)
33. Caprioli, M., Tarantino, E.: Accuracy assessment of per-field classification integrating very fine spatial resolution satellite imagery with topographic data. J. Geospat. Eng. **3**, 127–134 (2001)
34. Caprioli, M., Scognamiglio, A., Strisciuglio, G., Tarantino, E.: Rules and standards for spatial data quality in GIS environments. In: 21st Int. Cartographic Conf. Durban, South Africa, 10–16 August (2003)
35. Pengra, B., Long, J., Dahal, D., Stehman, S.V., Loveland, T.R.: A global reference database from very high resolution commercial satellite data and methodology for application to Landsat derived 30 m continuous field tree cover data. Remote Sens. Environ. **165**, 234–248 (2015)
36. Liang, S.: Narrowband to broadband conversions of land surface albedo I algorithms. Remote Sens. Environ. **76**, 213–238 (2000)
37. Smith, R.B. The heat budget of the earth's surface deduced from space (2010). Available on this site
38. Pindozzi, S., Cervelli, E., Capolupo, A., Okello, C., Boccia, L.: Using historical maps to analyze two hundred years of land cover changes: case study of Sorrento peninsula (south Italy). Cartogr. Geogr. Inf. Sci. **43**(3), 250–265 (2016)
39. Li, Y., Chen, J., Lu, R., Gong P., Yue, T.: Study on land cover change detection method based on NDVI time series batasets: change detection indexes design. In: IGARSS, pp. 2323–2326 (2005)